Precision Engineering 68 (2021) 126–138

Contents lists available at ScienceDirect

Precision Engineering

journal homepage: http://www.elsevier.com/locate/precision

Evaluation of surfaces complementarity based on high definition metrology

Yaxiang Yin [a,b], Kun Wang [a,b], Yiping Shao [c], Shichang Du [a,b,*], Lifeng Xi [a,b]

[a] State Key Lab of Mechanical System and Vibration, Shanghai Jiao Tong University, Shanghai, 200240, China
[b] School of Mechanical Engineering, Shanghai Jiao Tong University, No. 800 Dongchuan Road, Shanghai, 200240, China
[c] College of Mechanical Engineering, Zhejiang University of Technology, Hangzhou, China

ARTICLE INFO

Keywords:
Surfaces complementarity
Virtual assembly
High definition metrology
Sealing

ABSTRACT

The gap between two mating surfaces has a direct influence on sealing performance. However, traditional surface metrology rarely characterizes the gap between two mating surfaces. To solve this problem, a novel concept of surfaces complementarity is proposed in this paper. Surfaces complementarity measures how well two rough surfaces fit into each other. To make this concept applicable in engineering practices, a virtual assembly algorithm is developed. The automatic virtual assembly algorithm aligns the mating surfaces by maximizing the overlap ratio of the surface masks. Then, a sum surface which is complementary to the surface gap is constructed to represent the mating states. The top surface of a cylinder block and corresponding cylinder head surface measured by high definition metrology is mated by the virtual assembly algorithm. The differences of functional parameters between the mating surfaces and the sum surface are discussed thoroughly. Due to surfaces complementarity, parameters of the sum surface has a certain deviation from expected combined parameters from two individual surfaces. A case of square surface shows the practical application potential of the virtual assembly algorithm to optimize the sealing performance of the mating surfaces.

1. Introduction

Surface topography has a direct relationship with surface functions and surface manufacturing processes [1]. Among research about surface characterization, most papers aimed at process monitoring [2], since the initial goal of surface measurement was to help production engineers to improve process efficiency and quality assurance. Compared with the rich research about surface topography with its manufacturing processes, the relationship between surface functions and surface topography is still a challenge for surface metrologists. Surface topography has important influences on surface functions such as friction, wear and sealing, etc. [3]. Whitehouse utilized two independent variables to characterize surface functions: the normal separation of the two surfaces and the lateral relative velocity of the two surfaces [4]. For static sealing surfaces, since there is no relative motion between the two mating surfaces, the surface gap is the most important factor to determine the sealing performance besides the contact pressure and the sealing elements.

Although surface gaps are so important in surface function prediction, the practical difficulty is that surface gaps are not directly measureable. Most research about surface sealing adopt theoretical surface models without gaps measuring. For example, Bottiglione presented a theoretical model to estimate the fluid leakage in flat seals based on percolation scheme and fractal geometry [5,6]. Persson and Yang presented a critical junction theory to predict leak rate of seals based on contact mechanics and percolation theory [7]. Their theory shows that when two elastic solids with randomly rough surfaces are squeezed together, a non-contact channel will percolate when the relative contact area is of order 0.4. Lorenz and Persson compared effective-medium theory and critical junction theory with leakage experiment data and found good agreement between theories and experiments [8]. However, engineering surfaces produced by turning or milling are neither random nor fractal, thus violating the assumptions of the above leakage theories. In engineering practices, it is of great significance to estimate leakage based on the measured topography. Several efforts have been made to relate the surface topography with the sealing performance.

French automobile industry had developed a profile motif method to correlate the motif parameters to surface functions [9]. Numerous experiments showed the influence of motif roughness and waviness

* Corresponding author. State Key Lab of Mechanical System and Vibration, Shanghai Jiao Tong University, Shanghai, 200240, China.
E-mail addresses: yaxiang@sjtu.edu.cn (Y. Yin), wangkun1224@sjtu.edu.cn (K. Wang), syp123gh@zjut.edu.cn (Y. Shao), lovbin@sjtu.edu.cn (S. Du), lfxi@sjtu.edu.cn (L. Xi).

https://doi.org/10.1016/j.precisioneng.2020.12.006
Received 11 September 2020; Accepted 8 December 2020
Available online 11 December 2020

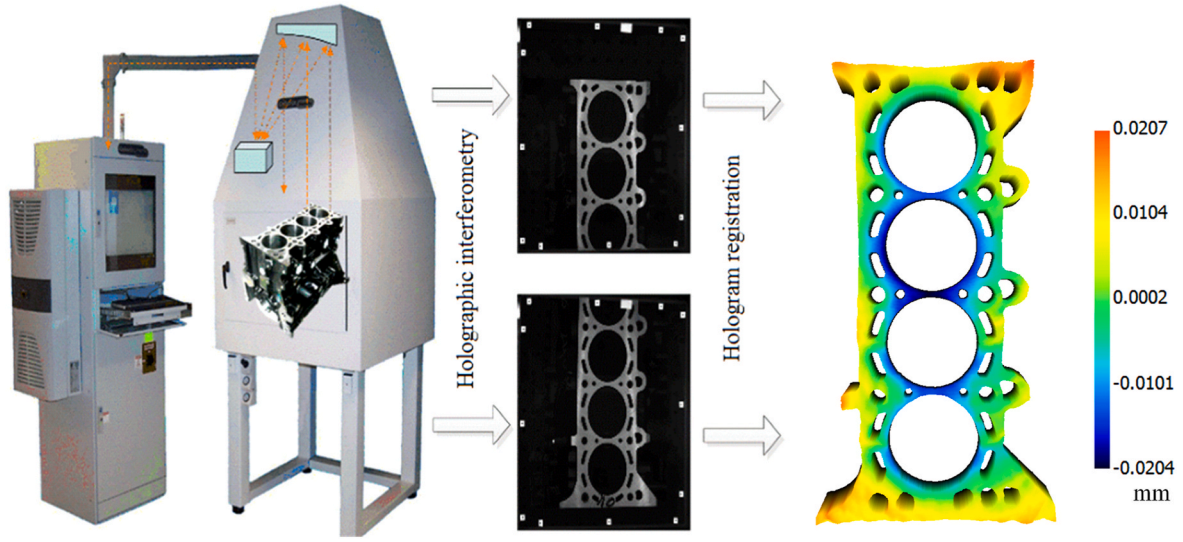

Fig. 1. Measurement by HDM

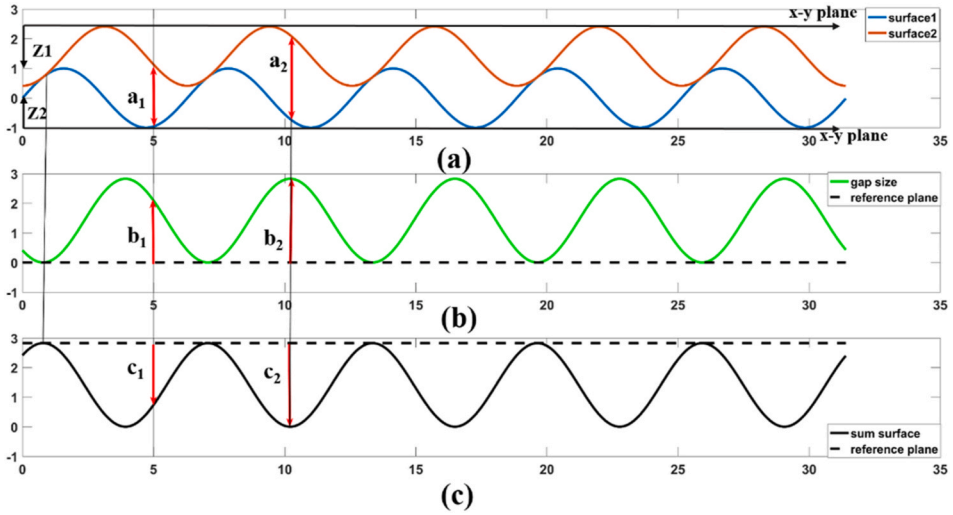

Fig. 2. Combination of two rough surfaces into one sum surface.

parameters to static sealing performances. F.Robbe-Valloire and M.Prat analyzed the face-turned surface microgeometry and found that the variability of valley altitudes has a significant impact to sealing performance. Malburg first proposed profile leakage parameters by simulating a virtual gasket on the waviness profile [10]. Since profile data is only a sample of the mating surfaces and may change with the sampling position, leakage prediction based on profile data is less reliable than surface topography data.

A recently developed high definition metrology (HDM) provides new opportunities to estimate sealing performance based on topography data of the full surfaces. Based on the principle of laser holographic interference, HDM could measure an engineering surface within 40s and generate millions of data points. For workpieces whose size exceeds the field of view, HDM could stitch multiple views to generate the full 3D height map of the surfaces. The HDM device and an engine block measured by HDM are shown in Fig. 1. Based on this novel measurement platform, some researches relating 3D surface topography to its sealing performance have been developed [11–13]. Based on HDM data, Shao et al. extended the concept of virtual gasket to three-dimensional (3D) cases and proposed areal leakage parameters [11]. Connectivity was included later to determine the leakage path [12]. Ren et al. considered the surface gap between the mating surfaces and proposed a stochastic model to predict the leakage area based on the leakage experiment data and a logistic regression method [13]. In Ren's model, the workpiece surfaces have a regular rectangle shape, so the surface gap could be calculated by simple algebraic operation.

For engineering surfaces with complex geometry such as the cylinder block and the cylinder head surfaces, there is a need of virtual assembly technology to align the mating surfaces. Virtual assembly is a method based on high precision model to simulate the positional relationship between the parts. Jayaram et al. first conducted the assembly accuracy analysis based on a virtual assembly design environment [14]. Zhong et al. constructed a meta-model for assembly tolerance types based on a description logic approach [15]. Gallegos-Nieto et al. presented a new haptic-enabled virtual assembly system to automatically generate and evaluate assembly plans [16]. However, little attention is paid to the virtual assembly of point clouds representing mating surfaces. To register the mating surfaces' height map into the same coordinate system, Zhang and Liu proposed an image guided point cloud registration method to virtually measure the car engine sealing states [17]. Zhang's method needs extra images and suitable feature lines selection to help the registration processes. If automation could be introduced into the

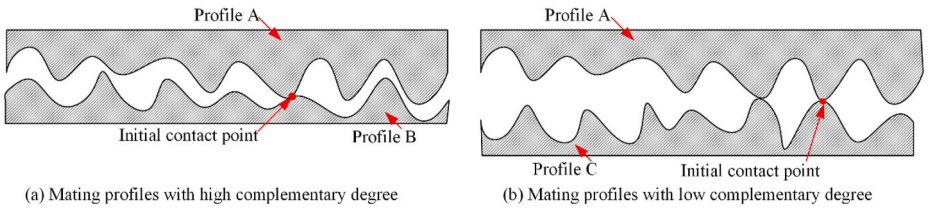

(a) Mating profiles with high complementary degree (b) Mating profiles with low complementary degree

Fig. 3. Mating profiles with different complementary degrees.

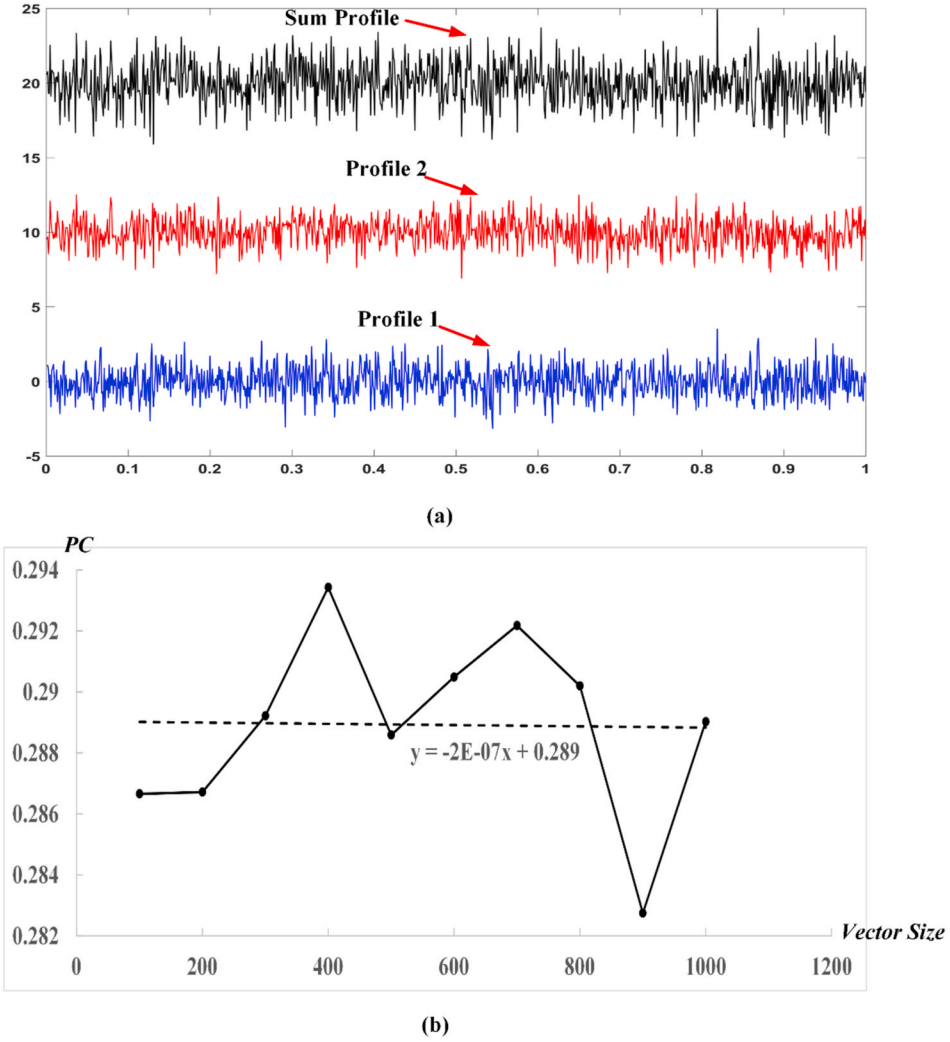

Fig. 4. Profile complementarities of simulated normal distributed profiles.

registration process, it will be more convenient to conduct the registration processes in engineering practices.

After registering the two mating surfaces, the surface gap could be calculated and the complement of the surface gap is the sum surface that could represent the assembly states of the mating surfaces. The complementary degree (termed as surfaces complementarity in this paper) of the mating surfaces have direct impacts on the related surface functions. Little research quantifies the surfaces complementarity. Moreover, the relationship between the surface gap (or the sum surface) and the original mating surfaces is rarely studied.

To fulfill the blank areas above, a formal quantitative definition of surfaces complementarity is proposed in this paper. An automatic virtual assembly algorithm is developed to align point clouds of engineering surfaces with complex geometries. With the aid of the automatic assembly algorithm, a thorough exploration of relationships between the sum surface and the original mating surfaces is conducted by case studies.

The rest of this paper is organized as follows. Section 2 first defines the concept of the sum surface and the surfaces complementarity. Then, the procedures of the automatic virtual assembly algorithm is described. Section 3 presents two case studies to explore the application potentials of the proposed concept of surfaces complementarity and the virtual assembly algorithm. Section 4 summaries this paper and gives the future research directions.

2. Methodology

2.1. Definition of the surfaces complementarity

Surfaces complementarity is determined by the mating gap of two

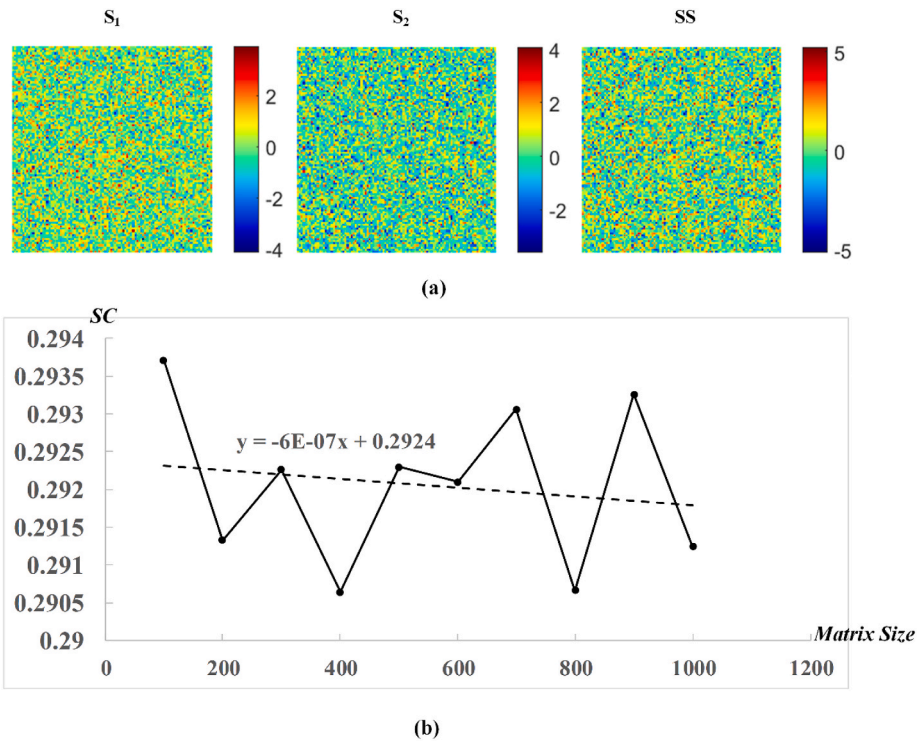

Fig. 5. Surface complementarities of simulated normal distributed surfaces.

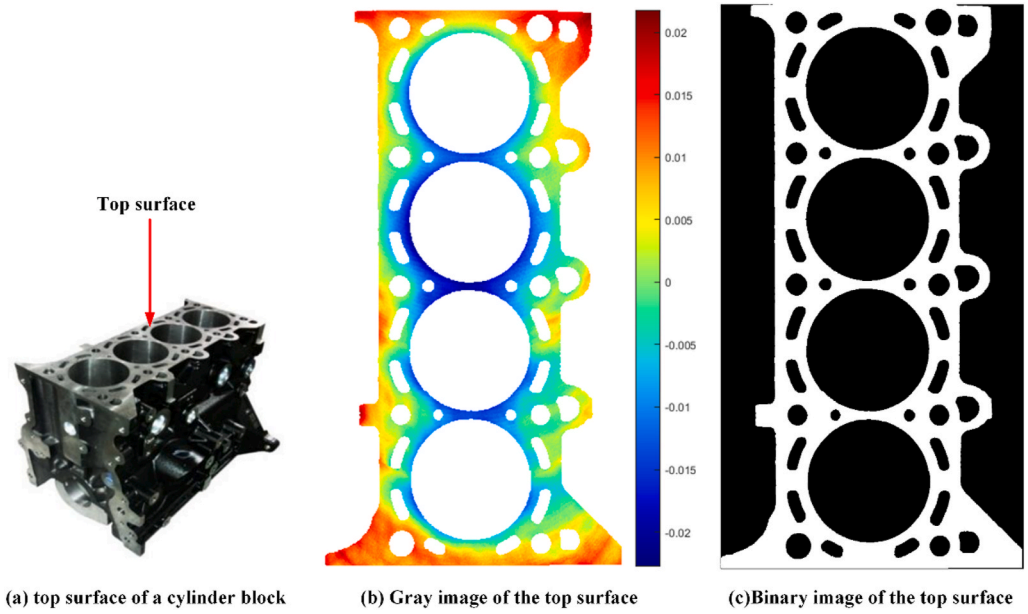

Fig. 6. Gray image and binary image of a cylinder block.

rough surfaces. Before formal definition of surfaces complementarity, the concept of surface gap and its complementary sum surface is illustrated first. In Fig. 2, the orange profiles z_1 and blue profiles z_2 represent two mating surfaces in an initial contact state. The normal distance between the two surfaces is shown by red double sided arrows in Fig. 2 (a). The green profile shown in Fig. 2(b) represents the gap size between the two surfaces. The red single sided arrows (represent the gap size) are the same length as the red double sided arrows in Fig. 2(a). It is clear that the gap or the normal distance of the two surfaces in initial contact can be defined as equation (1). The black profile in Fig. 2(c) represents the profile of the sum surface, which is complementary to the gap profile. The definition of the sum surface (*SS*) is equation (2).

$$d = \max(z_1 + z_2) - (z_1 + z_2) \tag{1}$$

$$SS = \max(d) - d = \max(d) - \max(z_1 + z_2) + (z_1 + z_2) = C + z_1 + z_2 \tag{2}$$

In equation (2), C is a constant, so the profile of sum surface is determined by adding of two mating surfaces as long as they are aligned. And the term of "sum surface" is also named by this relationship. The reference plane of the sum surface is the plane which is parallel to the mean line of the sum surface and passes through the highest point of the sum surface. The red arrows in Fig. 2(c) are the normal distance from

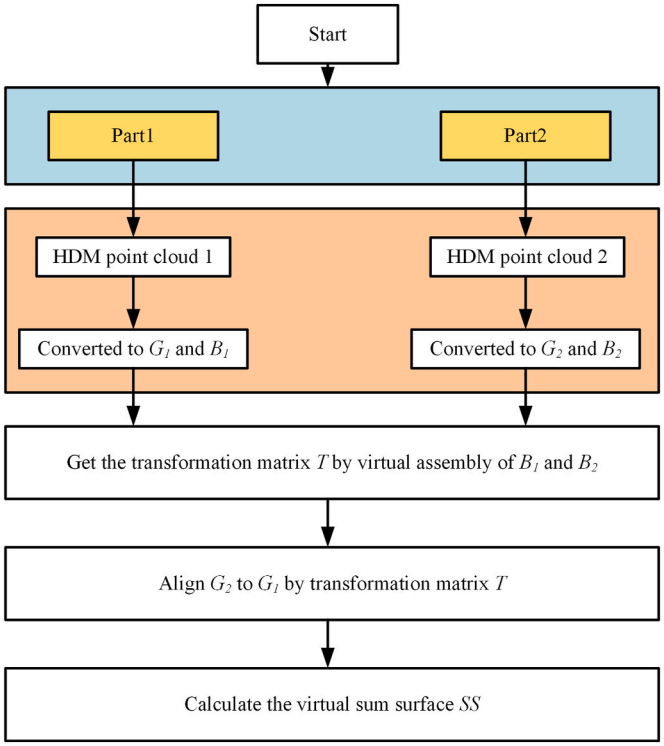

Fig. 7. Workflow of virtual assembling of mating surfaces.

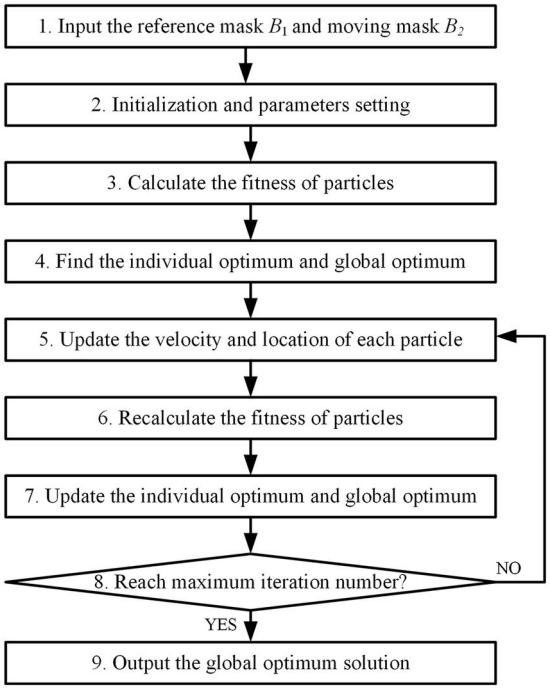

Fig. 8. Surface masks registration by the particle swarm optimization algorithm.

points of the sum surface to the reference plane. Obviously, $a_1 = b_1 = c_1$ and$a_2 = b_2 = c_2$. This relationship guarantees that the sum surface can keep the normal distance to reference plane the same as the normal distance of the original two rough surfaces in initial contact.

Huge differences of surface gap may occur when one surface is mated to different counter-surfaces as Fig. 3 shows. It is clear that profile B compensates profile A better than profile C. Moreover, the void area of the gap (VA_{gap}) between profile A and B is much smaller than the gap area between profile A and C. So the profile complementarity (*PC*) could be evaluated by the void area of profiles (VA_p) as equation (3), where *sp* is the abbreviation of sum profile, a similar concept of sum surface. Since the sum profile is complementary to the profile gap, $VA_{gap} = VA_{sp}$.

$$PC = 1 - \frac{VA_{gap}}{VA_{p_1} + VA_{p_2}} = 1 - \frac{VA_{sp}}{VA_{p_1} + VA_{p_2}} \tag{3}$$

$$VA_p = \int_p \max(P) - P(x)dx \tag{4}$$

Inspired by the observation of Fig. 3, the complementary degree *SC* between two mating surfaces S_1 and S_2 could be defined as equation (5) in a similar manner. VV_s denotes the void volume of a surface and is defined as equation (6). Since the sum surface is complementary to the surface gap, so the void volume of the gap VV_{gap} is equal to the void volume of the sum surface VV_{ss}. For two surfaces that are completely complementary to each other, the void volume of surface gap is zero, so the complementary degree *SC* is 1. For two surfaces with exactly mirrored surface topography, the volume of surface gap is equal to the summation of the void volume of each surface, the complementary degree *SC* is 0. Therefore, for engineering mating surfaces, their complementary degrees lie between 0 and 1. And the higher of *SC*, the better the mating surfaces compensate each other.

$$SC = 1 - \frac{VV_{gap}}{VV_{s_1} + VV_{s_2}} = 1 - \frac{VV_{ss}}{VV_{s_1} + VV_{s_2}} \tag{5}$$

$$VV_s = \iint_S (\max(S) - S(x,y))dxdy \tag{6}$$

For real engineering surfaces like Fig. 1, the surfaces are discontinuous with bores and holes. There is a modified surfaces complementarity defined with surface masks *B*. $B(x, y) = 1$ indicates that position (x, y) is a valid point on the surface, $B(x, y) = 0$ indicates that position (x, y) is not a valid point on the surface. Since the engineering mating surfaces are not exactly the same shapes, a unified surface mask $B(x, y) = B_1(x, y)$ & $B_2(x, y)$ is defined under the precondition that B_1 and B_2 have already been aligned correctly. And the surface gap and the sum surface are defined on positions where $B(x, y) = 1$, indicating that position (x, y) is valid on both mating surfaces. The void volume of the mating surfaces and the sum surface with surface masks are defined as equation (7), where the symbol "∘" represents a hadamard product. With the modified definition of void volume, the definition of surfaces complementarity keeps unchanged.

$$\begin{aligned} VV_{s_1} &= \iint_{s_1} [\max(S_1) - S_1(x,y)] \circ B(x,y)dxdy \\ VV_{s_2} &= \iint_{s_2} [\max(S_2) - S_2(x,y)] \circ B(x,y)dxdy \\ VV_{ss} &= \iint_{ss} [\max(SS) - SS(x,y)] \circ B(x,y)dxdy \end{aligned} \tag{7}$$

To illustrate the concept of surfaces complementarity more clearly, two examples are demonstrated. Two profiles of length *L* are simulated by equation (8), where *randn* is a function that returns numbers satisfying standard normal distribution. Fig. 4(a) shows the simulated profiles of length 1000 and the corresponding sum profiles. These three profiles are drawn at intervals in space to avoid overlapping. Let *L* varies from 100 to 1000 with a step size of 100, and for each *L* the simulation is repeated for 1000 times, then the average profile complementarities are calculated for each *L*. Fig. 4(b) shows the simulated *PC* values of different vector sizes. The average *PC* is 0.289 and the standard deviation is 0.0029. The linear trend line in Fig. 4(b) has a very small slope value. So it is inferred that for profiles satisfying normal distributions,

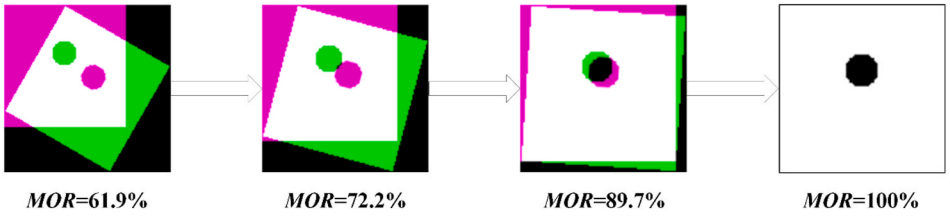

Fig. 9. The evolution processes of the automatic assembly algorithm.

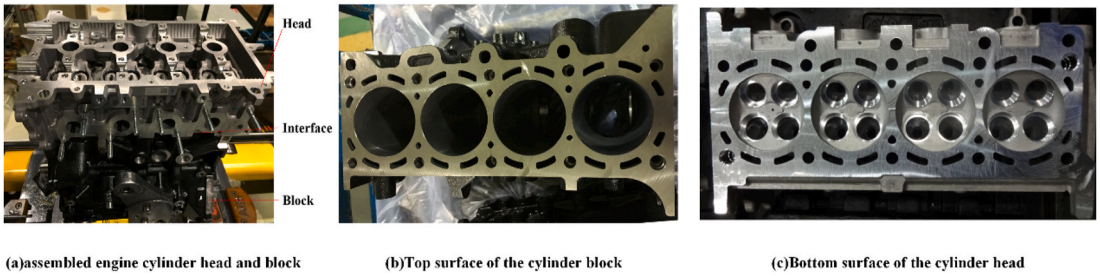

Fig. 10. The assembled engine and the two mating surfaces.

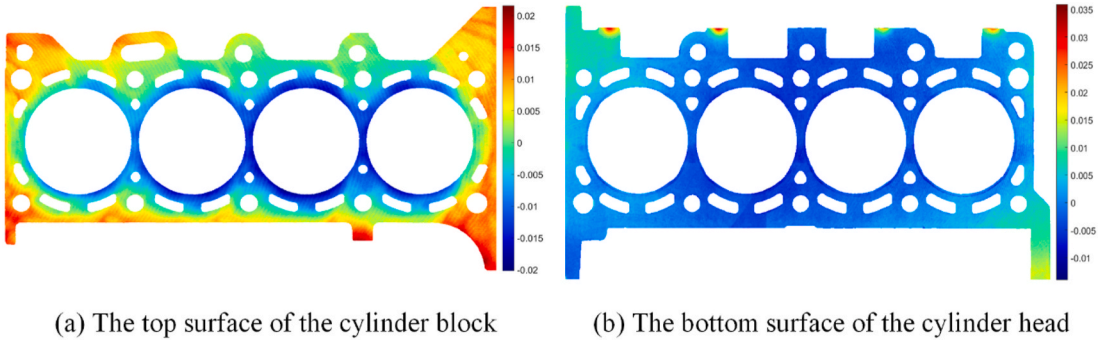

Fig. 11. The height map of the mating surfaces.

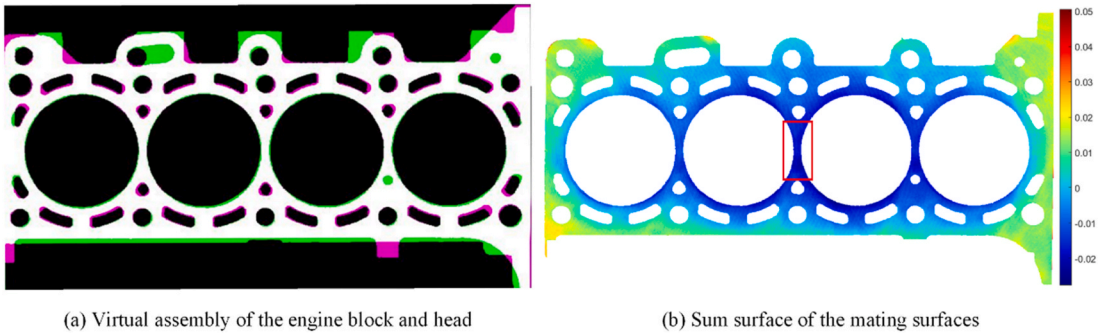

Fig. 12. Virtual assembly of the engine block and head.

their profile complementarities is a constant independent of profile length. The variation of *PC* values is due to the randomness of computer simulations.

$$z_1 = randn(L,1), \quad z_2 = randn(L,1), \quad SP = z_1 + z_2 \tag{8}$$

Surface simulation of similar manner is conducted by equation (9). Fig. 5(a) shows two simulated surfaces and the corresponding sum surface. The variation of L is the same as the profile simulations. The average SC is 0.292 and the standard deviation is 0.0010. The linear trend line in Fig. 5(b) also has a very small slope value, indicating that SC is independent of matrix sizes. Since normal distribution is a common assumption in surface simulations, the property that PC or SC is independent of profile or surface sizes is good. This property make it possible to compare the complementarities of profiles or surfaces of different sizes.

$$z_1 = randn(L,L), \quad z_2 = randn(L,L), \quad SS = z_1 + z_2 \tag{9}$$

2.2. Virtual assembly algorithm

Section 2.1 gives the formal definition of the sum surface and the surfaces complementarity under the precondition that the measurement

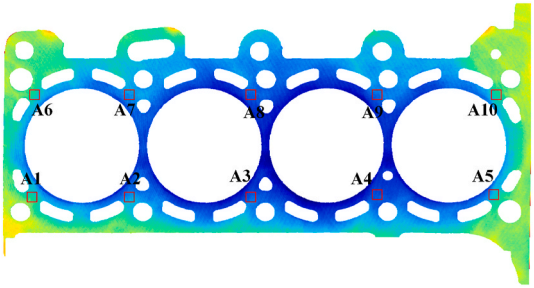

Fig. 13. Ten sampling regions of the mating surfaces.

Table 1
Difference of asperities' parameters.

Region	Diff(σ^2)	Diff(R)	Diff(η)	SC
1	0.575	0.486	0.387	0.172
2	0.312	0.331	0.547	0.096
3	0.176	0.222	0.520	0.116
4	0.226	0.344	0.391	0.296
5	0.060	0.092	0.520	0.185
6	0.258	0.434	0.411	0.034
7	0.101	0.185	0.439	0.031
8	0.162	0.382	0.493	0.19
9	0.046	0.236	0.396	0.319
10	0.559	0.327	0.421	0.206

data has already been aligned. However, in engineering practices, the alignment is not easy due to the complex geometry of real surfaces. This section presents the detailed algorithm to align the real engineering surfaces automatically based on HDM.

The HDM data of a planar surface could be converted to a height encoded gray image G and a binary image B (also called surface mask) using Wang's method [18]. $B(x, y) = 1$ if point (x, y) is on the surface, and $B(x, y) = 0$ otherwise. An example of the cylinder block surface is shown in Fig. 6. With two mating surfaces measured by HDM, the workflow to virtual assemble the mating surfaces is illustrated in Fig. 7. Different from traditional registration tasks where the images are taken from the same scene, the registration surfaces in this paper are from different workpieces. The surface topography from different workpieces has no correlations. Therefore, traditional registration method based on similarities of intensities cannot be applied directly. The critical skill in this virtual assembly algorithm is to register the surface masks instead of surface topography. The surface masks contain the important assembly features such as holes and bores and the physical assembly processes require the alignment of these holes and bores to realize the mechanical functions. The registration of surface masks simplifies the task of registration of surface topography, and the transformation matrix obtained from registration of surface masks could be used to register surface topography directly. Therefore, the most critical step in the workflow is get the transformation matrix by registration of surface masks. Once the transformation matrix is acquired, the gray image representing the mating surfaces' topography could be aligned and the sum surface could also be calculated.

When the two surface masks are aligned correctly, a maximum of masks overlap ratio (*MOR*) will occur. This property turns the surface masks registration task into an optimization problem. This optimization problem is described as follows:

$$\begin{aligned} \max\ & MOR(B_1,\ B_2(T(\Delta x, \Delta y, \theta))) \\ s.t.\ & -n \le \Delta x \le n \\ & -m \le \Delta y \le m \\ & 0 \le \theta < 2\pi \end{aligned} \tag{10}$$

$$MOR(B_1, B_2) = \frac{\sum_{i=1}^{m}\sum_{j=1}^{n}[if\ \ B_1(i,j) = B_2(i,j)\ 1\ \ else\ 0]}{mn} \tag{11}$$

where m and n are the row and column numbers of the reference surface mask B_1. $B_2(T)$ represents the surface mask transformed by matrix T. Since the surface masks are derived from real measurement data and the assembly parts have the same physical dimensions, the scaling factor is not included in the transformation parameters. Therefore, the transformation matrix T is determined by two translation factors Δx, Δy and a rotational angle θ as equation (12).

$$T(\Delta x, \Delta y, \theta) = \begin{bmatrix} cos\theta & sin\theta & 0 \\ -sin\theta & cos\theta & 0 \\ \Delta x & \Delta y & 1 \end{bmatrix} \tag{12}$$

To solve the optimization problem in equation (10), a particle swarm optimization (PSO) algorithm [19] is adopted to find the optimum transformation parameters (Δx, Δy, θ). PSO algorithm has the advantage of efficient global search capacity, fast search speed and simple structure. The procedures of using PSO algorithm to register the surface masks are shown in Fig. 8. Each step is detailed as follows.

Step1. Input the fixed surface mask B_1 as the reference image and a moving surface mask B_2 waiting to be registered with B_1. B_2 is up-down flipped to simulate the overturning operation in real assembly processes.

Step2. Set the acceleration constants, the boundary of particle positions and velocity, iteration number and population size, and randomly initialize the position x_k and velocity v_k of each particle.

Step3. Calculate the fitness of particles, and the fitness is the MOR value of transformed B_2 with B_1 (the transformation matrix is determined by the particle position).

Step4. For the first generation, the position of each particle is set as the initial p_{best} and the position with the maximum of fitness is set as the initial g_{best}. In each iteration of PSO evolution, p_{best} records the individual optimal position, g_{best} records the global optimal position.

Step 5. Update each particle and guide the particles to search the final global optimal position with the information of global optimal position

Table 2
Areal field parameters of the ten square samples.

Region	Sa(10^{-3}mm)			Sq(10^{-3}mm)			St(10^{-3}mm)		
	B	H	SS	B	H	SS	B	H	SS
1	1.361	0.705	1.791	1.700	0.880	2.247	8.604	5.270	11.772
2	1.677	0.636	2.043	1.995	0.781	2.448	8.708	4.014	11.287
3	1.600	0.444	1.776	1.892	0.546	2.125	8.893	3.072	10.112
4	0.691	0.421	0.835	0.834	0.524	1.025	4.287	3.344	5.682
5	2.364	0.486	2.566	2.909	0.630	3.181	13.940	3.595	15.052
6	1.405	0.579	1.794	1.708	0.731	2.206	8.533	4.377	10.797
7	1.083	0.590	1.291	1.286	0.745	1.565	6.375	4.536	9.538
8	1.150	0.438	1.249	1.385	0.553	1.537	7.073	3.390	7.720
9	1.204	0.451	1.405	1.419	0.561	1.631	6.586	3.396	7.622
10	1.042	0.548	1.426	1.306	0.686	1.797	8.295	3.824	10.518

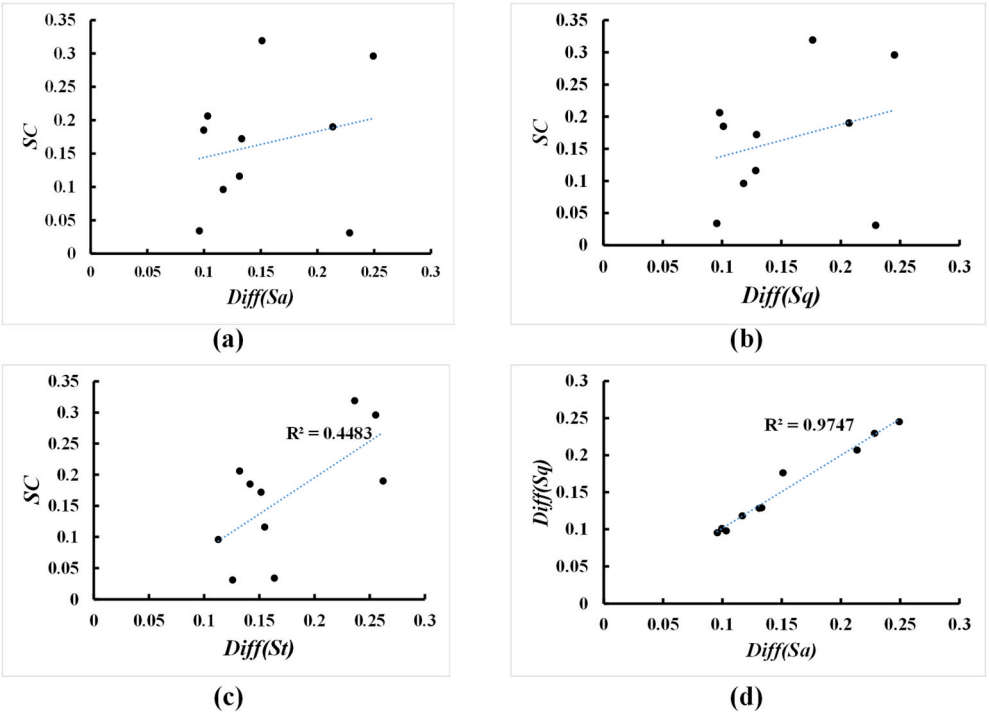

Fig. 14. Scatter plots of Diff(Sa), Diff(Sq), Diff(St) and SC.

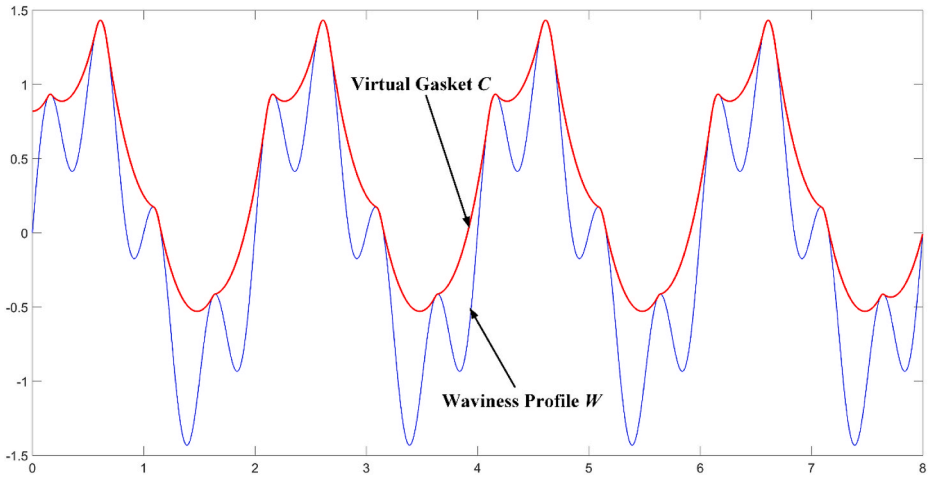

Fig. 15. Example of a waviness profile and its virtual gasket.

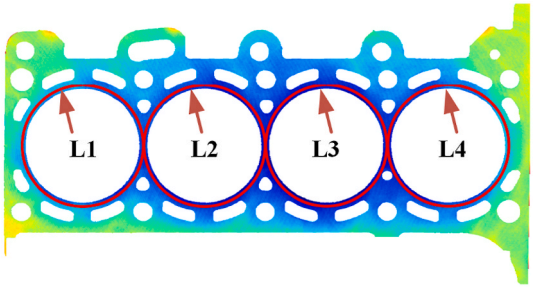

Fig. 16. Four line samples of the mating surfaces.

of current iteration and the historical local optimal position. The updating strategies of the velocity and position of each particle are the following equations:

$$v_{k+1} = \omega v_k + c_1 r_1 (p_{best} - x_k) + c_2 r_2 (g_{best} - x_k) \tag{13}$$

$$v_{k+1} = \begin{cases} v_{max} & v_{k+1} > v_{max} \\ -v_{max} & v_{k+1} \leq -v_{max} \end{cases} \tag{14}$$

$$x_{k+1} = x_k + v_k \tag{15}$$

where ω is the inertia weight, c_1 and c_2 are the acceleration constants, r_1 and r_2 are the random values sampled from [0,1], x_{k+1} is the current position of the particles that represents the transformation parameters.

Step6. Calculate the fitness of the updated particles.

Step7. Update the value of p_{best} and g_{best}.

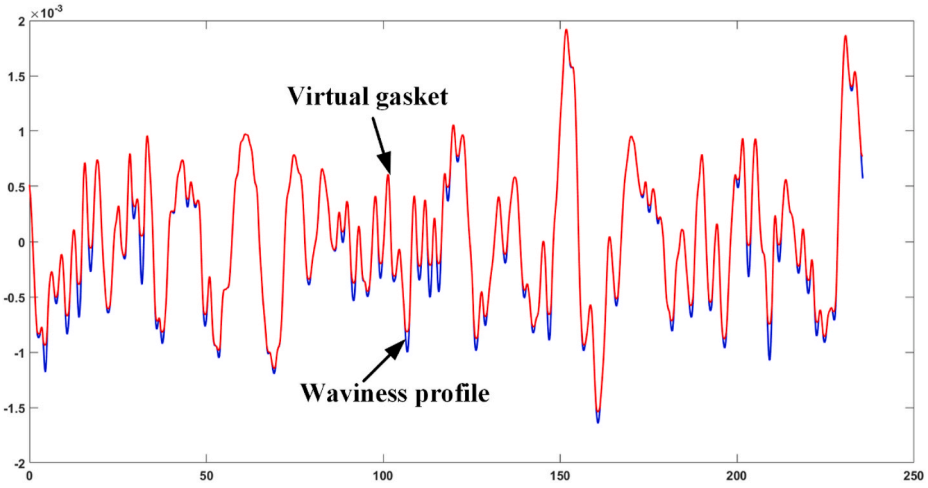

Fig. 17. Waviness profile and virtual gasket of L1 profile on the cylinder block.

Table 3
Leakage parameters of four samples on three surfaces.

Line	CLP			VA(10^{-3}mm^2)			SC
	B	H	SS	B	H	SS	
1	0.715	0.654	0.670	4.704	7.570	9.730	0.213
2	0.705	0.693	0.686	4.418	6.275	9.146	0.265
3	0.693	0.710	0.691	5.377	3.269	6.814	0.251
4	0.677	0.686	0.663	4.791	3.614	7.328	0.199

Step8. Check whether the maximum iteration number is reached. If the maximum iteration number is reached, go to Step9. Otherwise, go step5.

Step9. The algorithm terminates and output the global optimal solution (the transformation parameters which make the transformed B_2 has the maximum overlap ratio with B_1).

Fig. 9 shows an example of the evolution processes of the automatic assembly algorithm. By maximizing the MOR value, the masks tend to approach the correct assembly states.

3. Engineering case studies

3.1. Case study I

3.1.1. Virtual assembly of a cylinder block surface and a cylinder head surface

Leakage in an internal combustion engine is always an important issue. The contact states of the interface between the engine cylinder block and the cylinder head have direct relationships with its sealing performance. A conformable gasket is applied in the interface to prevent leakage. However, due to the form error of the two surfaces, gasket sometimes cannot fully fill the gap between the two mating surfaces. As a result, the leakage problem still happens in this interface sometimes. Once leakage problem occurs, it will bring many problems to the engine such as compression loss, power reduction and engine overheating or even cause the engine failure. In order to demonstrate the capacity of the proposed methodology for engineering practice, a case study on this interface is conducted.

The engine block and head in this case are from an automobile company. They are assembled by tightening 10 bolts, and the tight torque is 60Nm for each bolt. The assembled engine and two mating surfaces are shown in Fig. 10. The two surfaces were measured by ShaPix3D® 3000 series, with a vertical resolution of 0.05 μm and lateral resolution of 150 μm respectively. Its height measurement range is ±5 mm and the vertical accuracy is 1 μm. Its field of view is 280 mm × 280 mm, and the maximum number of sampling points is 4 million in each view. After preprocessing of the measurement data, the converted gray images which represent the height map of the surfaces are shown in Fig. 11. Applying the virtual assembly algorithm developed in section 2.2, the virtual assembly result and sum surface are shown in Fig. 12. The magenta regions in Fig. 12(a) are on the surface of the block but not on the surface of the head. And the green regions indicate the opposite cases. The sum surface is calculated on the white regions where both mating surfaces have valid data points as shown in Fig. 12(b). From Fig. 12(b), it is clear that the gap in the middle is bigger than all sides (low heights on the sum surface corresponding to big surface gap on the same position). Therefore, the connection part (labelled by a red box in Fig. 12(b)) between the second bore and the third bore has the highest risk of gas leakage. The same inference could be extended to other positions of interest.

3.1.2. Comparison with GT model

The concept of "sum surface" is not a new term in tribology. In 1970s, to calculate the contact properties between two rough surfaces, Greenwood and Tripp proposed the classical GT model [20]. This model constructs a sum surface by an equivalent relationship of asperity parameters, as equation (16) shows. σ^2 is the variance of the height distribution of the asperities, R is the average radius of the asperities and η is the distribution density of asperities.

$$\begin{cases} \sigma^2 = \sigma_1^2 + \sigma_2^2 \\ \dfrac{1}{R} = \dfrac{1}{R_1} + \dfrac{1}{R_2} \\ \eta = \eta_1 + \eta_2 \end{cases} \tag{16}$$

Since the concept of sum surface in GT model has been widespread, it is necessary to compare the statistical asperity parameters of the sum surface proposed in this paper to traditional GT model. Using the classical 9 PP-3D definition of asperity-peak [21], the asperity parameters can be calculated on 3D engineering surfaces. The radius R of the identified asperity-peak is calculated as the radius of a sphere that is fitted to the 9 points of the asperity peak according to the least-square method. Ten sampling regions are selected to compare the asperities' parameters of each mating surfaces and the sum surface (see Fig. 13).

The asperities parameters were calculated on the mating surfaces and corresponding GT equivalent parameters were obtained according to formula(16). The same parameters were calculated on the sum surface and compared to the GT model by equation (17). The difference of asperities' parameters predicted by GT model and calculated on the

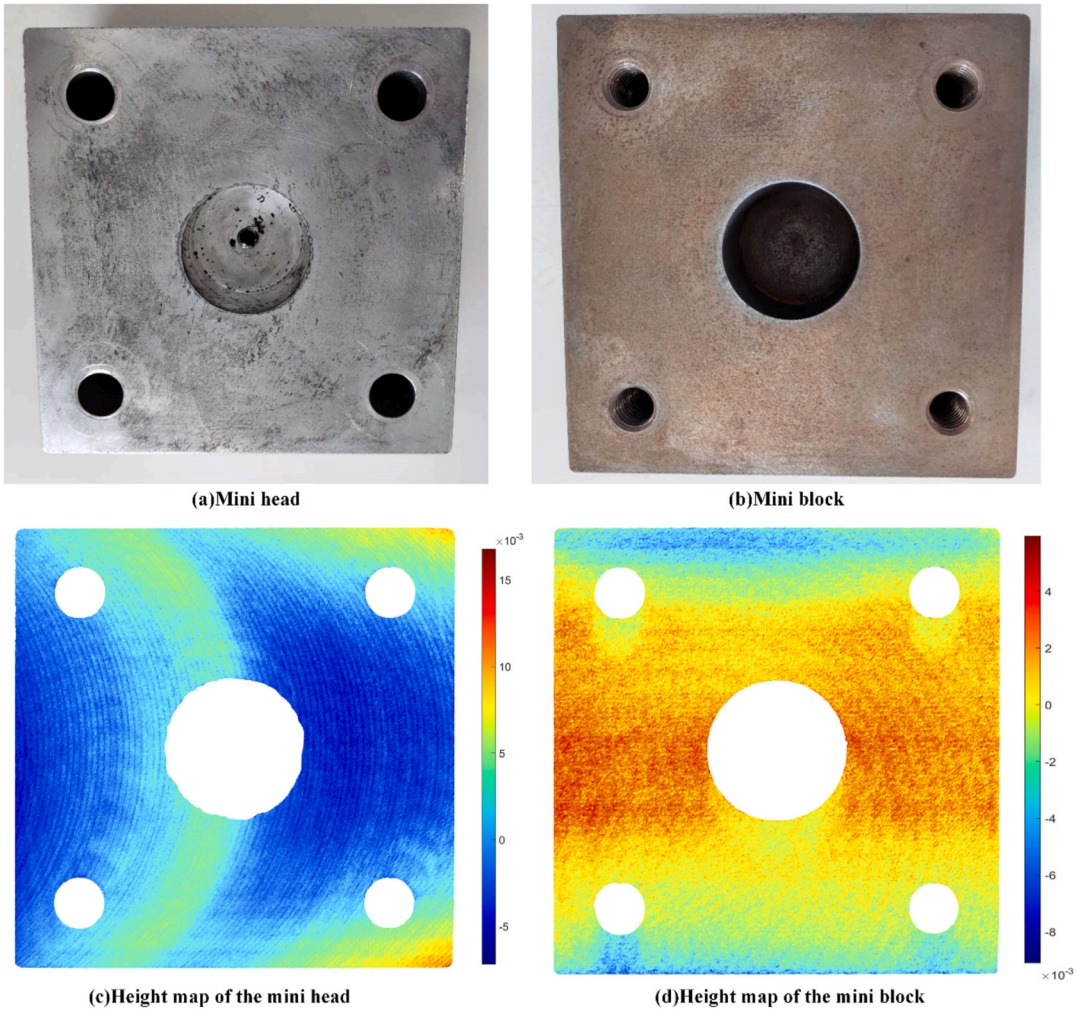

Fig. 18. The mini head and mini block and their height maps.

virtually assembled sum surface is listed in Table 1. The last column shows the surfaces complementarity of the ten regions. The mean difference of σ^2, R and η are 24.8%, 30.4% and 45.3% respectively. Such difference may due to the phenomenon of surfaces complementarity. The mean value of surfaces complementarity of the ten regions is 16.5%, very close to the half of mean difference of the three asperities' parameters.

$$\begin{cases} \mathrm{Diff}\left(\sigma^2\right) = \dfrac{\left|{\sigma^2}_{ss} - {\sigma^2}_{GT}\right|}{{\sigma^2}_{GT}} \\ \mathrm{Diff}(R) = \dfrac{|R_{ss} - R_{GT}|}{R_{GT}} \\ \mathrm{Diff}(\eta) = \dfrac{|\eta_{ss} - \eta_{GT}|}{\eta_{GT}} \end{cases} \tag{17}$$

3.1.3. Comparison of areal field parameters

The sum surface has a close relationship with its mating surfaces. It is interesting to explore the difference of some classical areal field parameters between the sum surface and the mating surfaces. In this section, three classical areal field parameters Sa, Sq, and St are computed on the ten square samples from the cylinder block (B), cylinder head (H) and the sum surface (SS). The definition of these three parameters are reviewed in equation (18). The values of the three parameters are listed in Table 2.

$$\begin{cases} Sa = \dfrac{1}{A}\iint_A |z(x,y)|dxdy \\ \mathrm{Sq} = \sqrt{\dfrac{1}{A}\iint_A z^2(x,y)dxdy} \\ \mathrm{St} = max(z) - min(z) \end{cases} \tag{18}$$

The difference of the three parameters between the sum surface and each individual surface is defined in equation (19).

$$\begin{cases} Diff(Sa) = \dfrac{Sa(B) + Sa(H) - Sa(SS)}{Sa(B) + Sa(H)} \\ \mathrm{Diff}(Sq) = \dfrac{Sq(B) + Sq(H) - Sq(SS)}{Sq(B) + Sq(H)} \\ \mathrm{Diff}(St) = \dfrac{St(B) + St(H) - St(SS)}{St(B) + St(H)} \end{cases} \tag{19}$$

The scatter plots of Diff(Sa), Diff(Sq), Diff(St) and SC are shown in Fig. 14. Diff(Sa) and Diff(Sq) have a strong linear correlation, and Diff (St) has an apparent positive correlation with SC. Generally, the higher of SC, the higher of Diff(Sa), Diff(Sq) and Diff(St), and the lower of Sa (SS), Sq(SS) and St(SS). The average value of Diff(Sa), Diff(Sq) and Diff (St) are 0.152, 0.152 and 0.174 respectively, while the average of SC is 0.165, approximately the average value of Diff(Sa), Diff(Sq) and Diff(St).

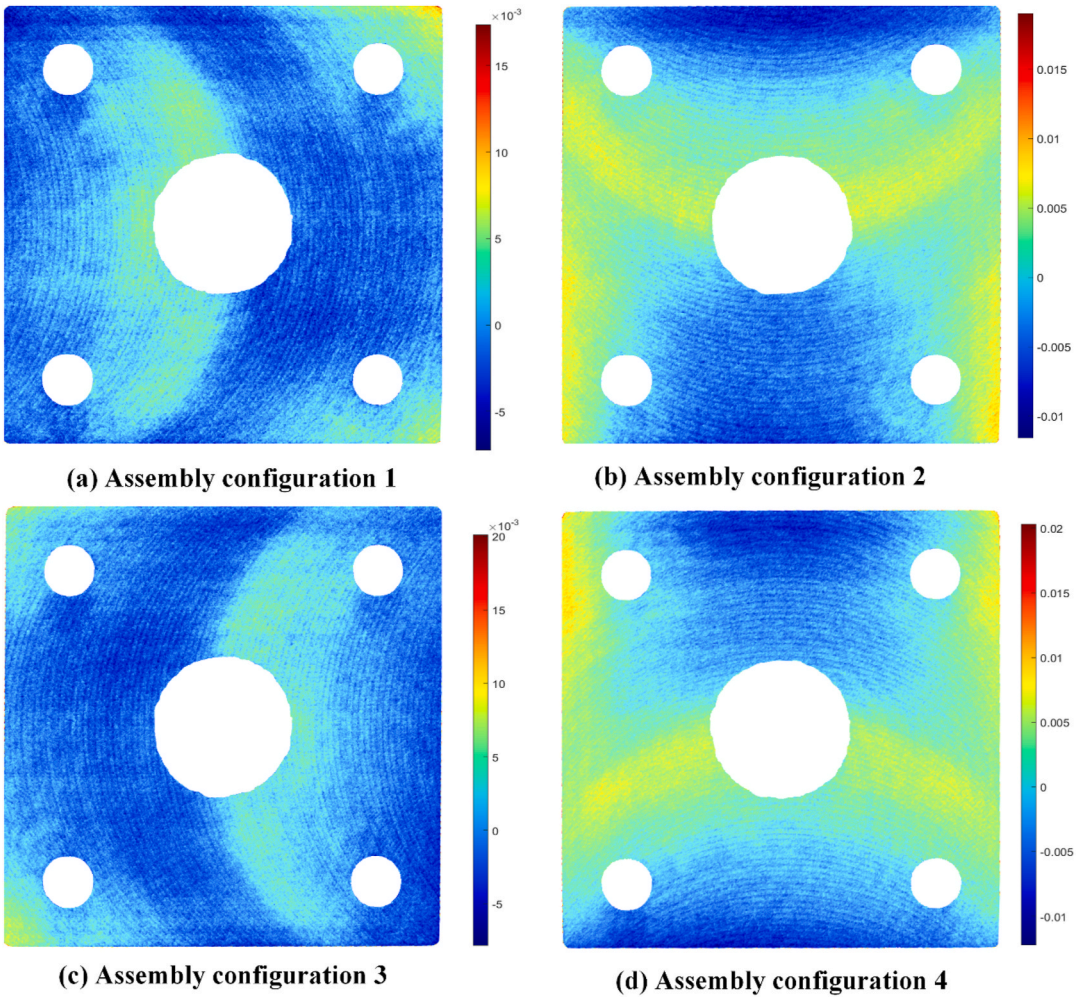

Fig. 19. Four types of assembly configuration.

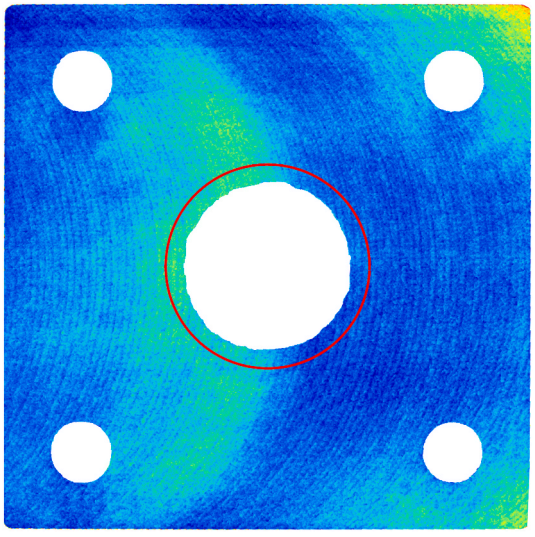

Fig. 20. Circle sampling of the mating surfaces.

3.1.4. Comparison of leakage parameters

Leakage is a major concern for the interface between cylinder blocks and cylinder heads. Traditionally, flatness is the main quality control parameter for surface mating in plant. However, even the two mating surfaces are within flatness tolerance, leakage may still occur when they are mated. In other words, individual quality control of each surface cannot guarantee the sealing performance of the mating interface. It is worthy to explore the difference of function predictions by individual surfaces and the sum surface which could represent the mating states. For leakage prediction, Malburg proposed three profile parameters to characterize the sealing capacity of the profiles [10]. The original profile was filtered to get the waviness component W, then a morphological closing filter is applied to simulate the virtual gasket C. Fig. 15 gives an example of a waviness profile and its virtual gasket. In this case, the

Table 4
Parameters of the mini block and mini head.

Parameters	Sa(mm)	Sq(mm)	St(mm)	CLP	VA(10^{-3}mm^2)
Mini block	0.0015	0.0019	0.0135	0.580	3.322
Mini head	0.0022	0.0027	0.0236	0.586	5.451

Table 5
Parameters of the four sum surfaces.

Assembly	Sa(mm)	Sq(mm)	St(mm)	CLP	VA(10^{-3}mm^2)	SC
1	0.0017	0.0021	0.0246	0.570	6.254	0.209
2	0.0031	0.0037	0.0306	0.562	6.430	0.134
3	0.0017	0.0021	0.0280	0.576	6.919	0.084
4	0.0031	0.0036	0.0326	0.562	7.261	0.075

contact length percentage (CLP) and void area (VA) are used to compare the difference between the two mating surfaces and the sum surface when predicting sealing performance. The definition of CLP and VA are reviewed in equation (20). Generally speaking, the larger of VA or the smaller of CLP, the worse of the profile sealing performance.

The surface topography around the bores is critical for sealing of engine combustion chamber. Four closed circles around the bores are selected to test the sealing capacity, as Fig. 16 shows. The circle sampled profiles are filtered by closed profile spline filter [22] to get the waviness profiles W (the low and high cut-off wavelength are 2.5 mm and 25 mm respectively), then waviness profiles are filtered by morphological closing with a circle of radius 3000 mm. Fig. 17 shows the waviness and virtual gasket of L1 profile on the cylinder block, and most of the waviness profile is in contact with the virtual gasket. The leakage parameters of four circle samples on the cylinder block (B), head (H) and sum surface (SS) are listed in Table 3. The last column shows the complementarity of each pair of circle samples.

$$\begin{cases} CLP = \dfrac{\sum_{n}[if(C_i = W_i)\ 1\ else\ 0]}{n} \cdot 100\% \\ VA = \displaystyle\int_0^l (C(x) - W(x))dx \end{cases} \tag{20}$$

From Table 3, it is clear that CLP is nearly the same between sum surface and each individual surface, since the virtual gasket could cover most of the profiles except for the deep valleys. Compared with the individual mating surfaces, the sum surface would have higher peaks and deeper valleys. VA considers the variation of depths of valleys, and from Table 3 it is also clear that $VA(SS) > VA(H), VA(B)$. Due to surfaces complementarity, $VA(SS) < VA(B) + VA(H)$. The difference of VA between the sum surface and each mating surfaces is defined as equation (21). The average Diff(VA) = 0.17, while the average SC = 0.23, close to the average Diff(VA).

$$Diff(VA) = \frac{VA(B) + VA(H) - VA(SS)}{VA(B) + VA(H)} \tag{21}$$

3.2. Case study II

An aluminum alloy block (called a mini head) and a cast iron block (called a mini block) are machined in laboratory to verify the applicability of the virtual assembly algorithm. These two surfaces are measured by ShaPix3D® 1500 series, with a vertical resolution of 0.05 μm and lateral resolution of 80 μm respectively. Its vertical accuracy is 1 μm and its field of view is 150 mm × 150 mm. The maximum number of sampling points is also 4 million in each view. The pictures of the mini head and the mini block are shown in Fig. 18(a) and (b) respectively. The gray images converted from the HDM data of the two mating surfaces are shown in Fig. 18(c) and (d) respectively. Since the mini block and mini head are the same shape when they are rotated by 90°, there are four types of assembly configurations. Fig. 19 shows the sum surfaces of the four types of assembly using the virtual assembly algorithm proposed in section 2.2.

To compare the difference among the mating surfaces and sum surfaces (four sum surfaces assembled by different orientations), three areal field parameters and two leakage parameters were calculated on these surfaces. The leakage parameters were calculated on a circle sample of the surfaces. The location and size of the sampling circle is shown in Fig. 20. The circle sampled profiles are filtered by closed profile spline filter to get the waviness profiles W (the low and high cut-off wavelength are 2.5 mm and 25 mm respectively). Then waviness profiles are filtered by morphological closing with a circle of radius 4000 mm. Parameters of the individual surfaces and the sum surface are listed in Table 4 and Table 5 respectively. From Table 5, it is clear that even the same surfaces will produce significantly different sum surfaces or surface gaps when mated with different orientations. Assembly by configuration 4 has the lowest surfaces complementarity and largest VA value, implying the worst sealing performance. In the contrast, assembly by configuration 1 has the largest surfaces complementarity and the smallest VA value, implying the best sealing performance. It is also noted that surfaces complementarity has a negative correlation with the VA values, indicating that SC could also be a good indicator for sealing performance.

4. Conclusion

This paper presents a new concept of surfaces complementarity (SC) which can measure how well two rough surfaces fit into each other. To make this new concept implementable in practice, a novel virtual assembly algorithm is proposed based on HDM. With this algorithm, the sum surface which is the complement of the surface gap could be constructed and the surfaces complementarity could be calculated. The first case of the interface between a cylinder block and a cylinder head shows the engineering application potential of the virtual assembly algorithm. The concept of sum surface is compared with traditional GT model by numerical asperity parameters, and the result shows the real sum surface has a certain deviation with GT model due to the phenomenon of surfaces complementarity. Areal field parameters comparison shows that the higher of the surfaces complementarity, the lower of the Sa, Sq and St value of the sum surface. Leakage parameters comparison shows that variation of VA has a closed relationship with surfaces complementarity. A case study of the square surfaces shows the practical application potential of the virtual assembly algorithm to optimize the sealing performance of the mating surfaces.

Declaration of competing interest

The authors declare that they have no known competing financial interests or personal relationships that could have appeared to influence the work reported in this paper.

Acknowledgements

This work was supported by the National Natural Science Foundation of China (Grant No. 51775343 and No. 51535007).

References

[1] Whitehouse D. Handbook of surface and nanometrology. second ed. University of Warwick Coventry,UK: CRC Press; 2002.
[2] Cabuil N, Le Gouil A, Doclot O, Dickson B, Lagha A, Aminpur M, Chaton C, Royer JC. Process monitoring and surface characterization with in-line XPS metrology. Solid State Technol 2007;50:48–51.
[3] Lorenz B, Persson BNJ. On the dependence of the leak rate of seals on the skewness of the surface height probability distribution. Europhys Lett 2010;90(3).
[4] Whitehouse DJ. Function maps and the role of surfaces. Int J Mach Tool Manufact 2001;41(13):1847–61.
[5] Bottiglione F, Carbone G, Mangialardi L, Mantriota G. Leakage mechanism in flat seals. J Appl Phys 2009;106(10).
[6] Bottiglione F, Carbone G, Mantriota G. Fluid leakage in seals: an approach based on percolation theory. Tribol Int 2009;42(5):731–7.
[7] Persson BNJ, Yang C. Theory of the leak-rate of seals. J Phys Condens Matter 2008; 20(31).
[8] Lorenz B, Persson BNJ. Leak rate of seals: effective-medium theory and comparison with experiment. Eur Phys J E 2010;31(2):159–67.
[9] ISO. Geometrical product specifications(GPS)-Surface texture: profile method-motif parameters. Geneva,Switzerland: International Organization for Standardization; 1996. Standard No. ISO 12085:1996.
[10] Malburg MC. Surface profile Analysis for conformable interfaces. J Manuf Sci Eng 2003;125(3):624–7.
[11] Shao YP, Yin YX, Du SC, Xia TB, Xi LF. Leakage monitoring in static sealing interface based on three dimensional surface topography indicator. ASME Trans Manufac Sci Eng 2018;140:101003.
[12] Shao YP, Yin YX, Du SC, Xi LF. A surface connectivity based approach for leakage channel prediction in static sealing interface. J Tribol 2019;141(6):062201.
[13] Ren J, Park C, Wang H. Stochastic modeling and diagnosis of leak areas for surface assembly. J Manuf Sci Eng 2018;140(4):041011.
[14] Jayaram S, Yong W, Jayaram U, Lyons K, Hart P, A virtual assembly design environment, Proceedings IEEE virtual reality (cat. No. 99CB36316), 172-179.

[15] Zhong Y, Qin Y, Huang M, Lu W, Chang L. Constructing a meta-model for assembly tolerance types with a description logic based approach. Comput Aided Des 2014; 48:1–16.
[16] Gallegos-Nieto E, Medellin-Castillo Hugo I, Xiu-Tian Y, Corney J. Haptic-enabled virtual planning and assessment of product assembly. Assemb Autom 2020;40(4): 641–54.
[17] Zhang X, Liu H. Image guided as-assembled car engine sealing surface modeling. In: International conference on robotics and automation engineering; 2017. p. 317–21.
[18] Wang M, Xi LF, Du SC. 3D surface form error evaluation using high definition metrology. Precis Eng 2014;38(1):230–6.
[19] Eberhart R, Kennedy J, A new optimizer using particle swarm theory, MHS'95. Proceedings of the sixth international symposium on micro machine and human science, 39-43.
[20] Greenwood JA, Tripp JH. The contact of two nominally flat rough surfaces. Proc Inst Mech Eng 1970;185(1):625–33.
[21] Kalin M, Pogačnik A. Criteria and properties of the asperity peaks on 3D engineering surfaces. Wear 2013;308(1):95–104.
[22] Krystek M. Form filtering by splines. Measurement 1996;18(1):9–15.